



Pappas, A., Sextos, A., Da Porto, F., & Modena, C. (2017). Efficiency of alternative intensity measures for the seismic assessment of monolithic free-standing columns. *Bulletin of Earthquake Engineering*, 15(4), 1635-1659. <https://doi.org/10.1007/s10518-016-0035-0>

Publisher's PDF, also known as Version of record

License (if available):  
CC BY

Link to published version (if available):  
[10.1007/s10518-016-0035-0](https://doi.org/10.1007/s10518-016-0035-0)

[Link to publication record in Explore Bristol Research](#)  
PDF-document

This is the final published version of the article (version of record). It first appeared online via Springer at DOI: 10.1007/s10518-016-0035-0. Please refer to any applicable terms of use of the publisher.

## University of Bristol - Explore Bristol Research

### General rights

This document is made available in accordance with publisher policies. Please cite only the published version using the reference above. Full terms of use are available:  
<http://www.bristol.ac.uk/red/research-policy/pure/user-guides/ebr-terms/>

# Efficiency of alternative intensity measures for the seismic assessment of monolithic free-standing columns

Athanasios Pappas<sup>3</sup> · Anastasios Sextos<sup>1,2</sup> · Francesca da Porto<sup>3</sup> · Claudio Modena<sup>3</sup>

Received: 10 June 2015 / Accepted: 3 October 2016 / Published online: 26 October 2016  
© The Author(s) 2016. This article is published with open access at Springerlink.com

**Abstract** This paper deals with the dynamic response of a free-standing ancient column in the Roman Agora of Thessaloniki, Greece as a means to shed more light on the complex behaviour of rocking bodies under seismic excitation. Numerical analyses utilizing discrete element method were carried out with the use of multiple seismic records selected based on the disaggregation of the seismic hazard for the region of interest. To identify their impact on structural performance, earthquake Intensity Measures, such as Peak Ground Acceleration and Peak Ground Velocity are examined for the case of a column that sustained no visible permanent deformations during the  $M_s = 6.5$  Thessaloniki earthquake of 1978. The analysis revealed a weak correlation of PGA and PGV with the response results and a significant influence of the mean frequency ( $f_m$ ) of the seismic motion. No coupling was found between the maximum displacement of the top during the oscillation and the permanent post-seismic deformations. The complementarity of both earthquake Intensity Measures in the structural vulnerability assessment is also depicted.

**Keywords** Ancient monuments · Free standing column · Rocking · Discrete element method (DEM) · Seismic vulnerability · Intensity measures

## 1 Introduction

A free-standing column is a rather simple structural element which, due to its ability to perform rocking oscillations, has a disproportionally complex behaviour when subjected to earthquake ground motions (Housner 1963; Yim et al. 1980). The reason is that, in addition

---

✉ Anastasios Sextos  
a.sextos@bristol.ac.uk

<sup>1</sup> Department of Civil Engineering, University of Bristol, Bristol BS8 1TR, United Kingdom

<sup>2</sup> Department of Civil Engineering, Aristotle University of Thessaloniki, Thessaloniki, Greece

<sup>3</sup> Department of Civil, Architectural and Environmental Engineering, University of Padova, Padua, Italy

to the intrinsic properties of the column, the frequency content, duration and amplitude of the earthquake excitation may also greatly influence its structural response. As in the case of conventional modern structures therefore, much research has been devoted to the proper selection of earthquake records (Katsanos et al. 2010; Sextos et al. 2011) and the efficiency of different Intensity Measures (IM) that are commonly used in the framework of seismic vulnerability assessment (Shome and Cornell 1999).

One of the most widely used, though preliminary, selection criteria is the earthquake Magnitude (M) and source-to-site distance (R) of the rupture zone (Stewart et al. 2001; Bommer and Acevedo 2004). Studies, however, have questioned the dependency of the structural response quantities on the M-R pairs (Shome and Cornell 1998; Iervolino and Cornell 2005). Similarly, Psycharis et al. (2013) studied the effect of magnitude and distance on a multi-drum free-standing column, and interestingly, it was found that for some distances, the structural response in terms of displacement and final dislocation was not correlated with increasing magnitude. Other complementary selection criteria include the soil profile, which may alter and/or amplify response spectra at specific periods of interest (Bommer and Acevedo 2004) and the strong motion duration causing damage accumulation (Iervolino et al. 2006). Spectral matching between a target spectrum and the response spectrum (Bommer et al. 2003; Ambraseys et al. 2004), which can also take into account the spectral shape (Baker and Cornell 2005; Mousavi et al. 2012), may also be used for assessment of seismic vulnerability. The spectral shape is considered by means of the parameter “epsilon” (“ $\epsilon$ ”) that expresses the number of standard deviations by which a given IM differs from the mean predicted IM value, where both values are expressed in logarithmic terms. The spectral matching can take place either using the Uniform Hazard target Spectrum (UHS), which represents the locus of points such that the spectral acceleration at each period has a specific (and uniform) exceedance probability, or the Conditional Mean Spectrum (CMS) which provides the expected response spectrum conditioned on occurrence of a target spectral acceleration value at a single period of interest (Baker 2011). Notwithstanding the major advancement made by means of CMS, limitations also apply since CMS matching is based on the predominant target period, typically the fundamental vibration period of the structure, which is not defined for the case of rocking elements whose (instantaneous) fundamental period evolves in time (Housner 1963).

Based on analytical formulations and extended simulations, Ishiyama (1984) proposed that for rocking bodies, both ground velocity and ground acceleration has to be taken into account for assessing the dynamic response. This work also proposed an empirical value of period which, for shorter periods of excitation, leads to acceleration demand that significantly increases overturning susceptibility. It is well known that rocking structures are also particularly vulnerable to long-period ground motions and more precisely, to the persistence of the pulse (Ishiyama 1984; Spanos and Koh 1984; Augusti and Sinopoli 1992; Manos and Demosthenous 1996; Konstantinidis and Makris 2005; Manos et al. 2013). In tall buildings, which are similarly vulnerable to long periods, the Peak Ground Velocity (PGV) was found to be a more efficient IM compared to the Peak Ground Acceleration (PGA) or Spectral acceleration ( $S_a$ ) (Sehhati et al. 2011).

The proper choice of a representative IM has also been found to depend on the type of ground motion under consideration. Near-field and especially forward-directivity motions cause a distinct high intensity velocity pulse at the beginning of the record (Gabor 1946), which may cause rocking and overturning to free-standing structures. Attenuation relationships are available for correlation of multiple seismological parameters to the PGV and dominant pulse period (Mavroeidis and Papageorgiou 2003; Bray and Rodriguez-Marek

2004). Acikgoz and DeJong (2012) used near-field records to study the effect of low frequency on the rocking behaviour of large flexible structures during certain earthquakes. This work demonstrated that seismic records characterised by low frequency velocity pulses produce a similar rocking response despite of a significantly varying PGA. Many studies however, (Psycharis et al. 2000; Papantonopoulos et al. 2002; Psycharis et al. 2003; Papaloizou and Komodromos 2009; Yagoda-Biran and Hatzor 2010; Dimitri et al. 2011; Pappas et al. 2016) focused on the seismic vulnerability of rocking bodies using only the PGA as IM, while in recent works (Psycharis et al. 2013) a comparison between PGA and PGV was also attempted for assessing their reliability in expressing ground motion intensity. All studies mentioned above are effectively in agreement with the early proposal of Yim et al. (1980) according to which, it is necessary to adopt a probabilistic approach to study rocking behaviour.

Given the above extensive but rather inconclusive research results, the scope of this paper is to shed some light on the implications in selecting an efficient IM for studying rocking bodies under seismic excitation. The attention is drawn on the earthquake-induced ground motion because, compared to other uncertainties stemming from the material properties (joint friction, mechanical properties of the column), seismic motion has by far the most significant impact on the variability observed in the structural response for free-standing rocking structures (DeJong 2009; Dimitri 2009; Psycharis et al. 2013). For this purpose, the efficiency of PGA and PGV to predict the structural response of free-standing columns was assessed based on their correlation analysis with the numerical outputs for the case of an ancient Roman column that was simulated with the Discrete Element Method (DEM). The column was subjected to dynamic analysis with carefully selected seismic records and correlation patterns were sought. The methodology adopted and the observations made are presented and discussed in the following sections.

## 2 Overview of the case studied

The column under study is located in the ancient Roman Agora of Thessaloniki, Greece. The site was brought to light after the first excavations of 1962 (Adam-Veleni 2001) and was re-established in 1969 (Fig. 1). The column shaft is made of a single monolithic body with cylindrical section without fluting. The height of this block is 6.0 m and has a constant diameter of 0.66 m (Fig. 2). The capital has an additional height of 0.8 m and the diameter on the top is 0.9 m. The overall height divided by the diameter corresponds to a

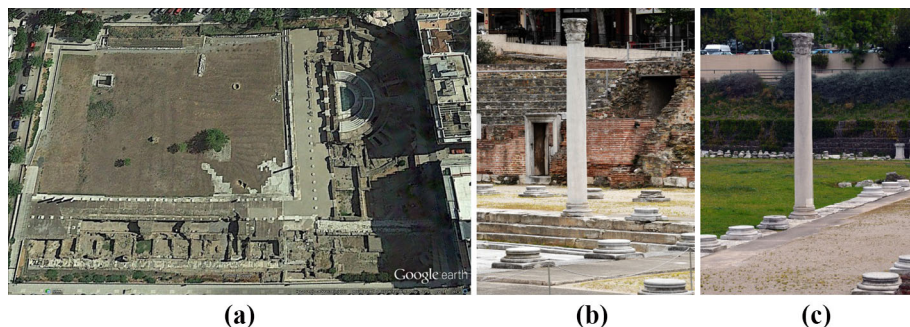


**Fig. 1** Ancient Agora of Thessaloniki archaeological site (a), free-standing Roman column overview (b), (c)

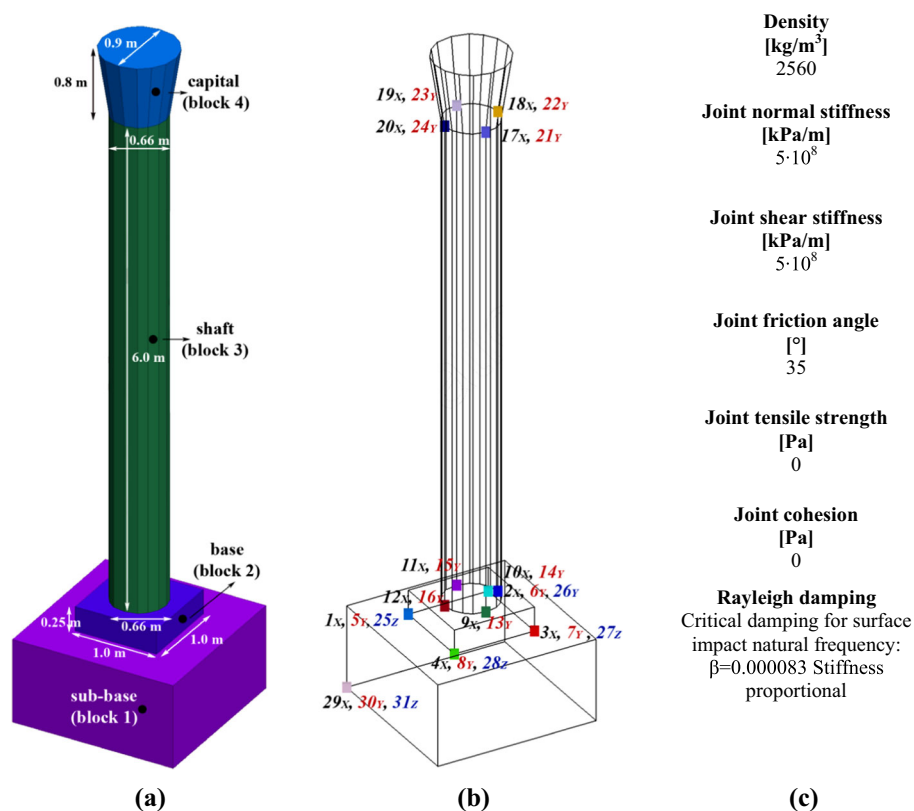


**Fig. 2** Numerical model and dimensions (a); position of the control points (b) and model parameters

slenderness ratio of 10.3 (Sextos et al. 2013). The column is positioned on a square base of edge 1.0 m and height 0.34 m. The vulnerability assessment of the column is performed using earthquake records that correspond to realistic seismic scenarios for the examined area. The fact that the column resisted the strong ( $M_s = 6.5$ ) earthquake of 1978 without any visible permanent dislocation or rotation triggered the interest to investigate the result that different seismic records would produce in terms of residual deformations.

### 3 Methodology

#### 3.1 Seismic record inputs

To understand the influence of the main ground motion characteristics on the structural response, earthquake records with specific characteristics of PGA, PGV and mean period ( $T_m$ ) were selected. The numerical analyses were carried out using all 3 components of ground motions, retrieved from PEER-NGA database (Stewart et al. 2001). Yim et al. (1980) yielded that the vertical component of the seismic excitation affects the overturning but in no systematic way, hence, although the vertical component was taken into account in all analyses, its influence was not further studied in this paper.

Preliminary characteristics for selecting earthquake records were based on disaggregation of seismic hazard for the city of Thessaloniki (Pitilakis et al. 2007) being compatible to magnitude  $6.0 < M < 6.5$ , source-to-site distance  $10 \text{ km} < R < 30 \text{ km}$  and average  $30 \text{ m}$  shear wave velocity  $200 \text{ m/s} < V_{s,30} < 300 \text{ m/s}$ . The ground motion recorded during the Thessaloniki earthquake of 20/06/1978, a shallow depth, normal event of  $M_s = 6.5$  magnitude, which was generated by a blind fault at a source distance of 8–10 km from the city centre, was also included in the ensemble. The particular motion was recorded during the main shock at the basement of the City Hotel located at a distance of only 900 m from the Ancient Agora, and is characterised by  $\text{PGA} = 0.15 \text{ g}$ ,  $\text{PGV} = 0.14 \text{ m/s}$  and  $T_m$  approximately between 0.4 and 0.5 s.

It is recalled, that the mean period of the ground motions  $T_m$  is derived by weighting the amplitudes over a specified range of the Fourier Amplitude Spectrum (Rathje et al. 2004):

$$T_m = \frac{1}{f_m} = \frac{\sum c_i^2 \frac{1}{f_i}}{\sum c_i^2} \quad (1)$$

where  $c_i$  are the Fourier amplitude coefficients and  $f_i$  are the discrete fast Fourier transform (FFT) frequencies between  $0.25 \text{ Hz} \leq f_i \leq 20 \text{ Hz}$  and  $\Delta f \leq 0.05 \text{ Hz}$  is the frequency interval used in the FFT.

It is also noted that  $T_m$  is not necessarily a representative indicator of the persistence of the pulse along the entire period range, which has been shown to be a more efficient IM in terms of free body rocking (Vassiliou and Makris 2011). However, it is used herein as a means to select ground motions that match the (uniform hazard) code-defined spectrum, thus providing equal probability of exceedance at all structural periods at the site of interest. Given the above criteria, ground motion selection has been performed using the PEER-NGA compatible computer program ISSARS (Katsanos and Sextos 2013). The ensemble of motions formed is summarised in Table 1 along with the column Engineering Demand Parameter (EDP) of interest, in this case, displacement of the highest point of the shaft normalised to the displacement capacity. For clarity, only the horizontal components of the records are presented in Table 1.

### 3.2 Discrete element model description

Herein, the numerical modelling of the structure was based on the Discrete Element Method (DEM) introduced by Cundall (1976). DEM, regards the structure as an assembly of discrete blocks and the solution is based on a time algorithm of sufficiently small time-steps. The solution scheme is described by Cundall (1976) as the DEM cycle. The cycle consists firstly on the calculation of the block motion in terms of velocity and acceleration, which are assumed to be constant within a given time-step. As the blocks move relatively, new contacts between blocks are detected and the relative contact velocities and forces are updated with the use of a force–displacement law. Finally, the new forces for each block centroid are calculated and the new block motion is updated with the application of Newton’s second law. The method is particularly efficient for reproducing the seismic response of rigid bodies, which is characterised by large displacements and rotations (Papantonopoulos et al. 2002; Lemos 2007).

The numerical model of the structure was developed with the use of the DEM software 3DEC (Itasca Inc. 2013). All column blocks were modelled as rigid using the specific weight for marble,  $2560 \text{ kg/m}^3$ . The Coulomb friction law was implemented for the joints between blocks with zero cohesion and an angle of friction equal to  $35^\circ$  ( $\mu = 0.7$ ) (Dimitri

**Table 1** Horizontal components of the earthquake records used for dynamic analysis and associated dynamic response of the column under study

Earthquake characteristics											
#	Earthquake record	PGA (SRSS <sup>a</sup> ) (g)	PGV (SRSS) (m/s)	Mean Frequency f <sub>m</sub> (Hz)	PGA (RES <sup>b</sup> ) (g)	PGV (RES) (m/s)	Horizontal components	PGA (g)	PGV (m/s)	Mean Period T <sub>m</sub> (s)	Frequency f <sub>m</sub> (Hz)
0.10 g < PGA < 0.25 g											
0	THESS_CITY78	0.197	0.169	3.09	0.173	0.141	THESS_CITY_X	0.133	0.096	0.25	4.00
							THESS_CITY_Y	0.146	0.139	0.46	2.17
19	CHALFANT_A-SHE	0.187	0.089	5.84	0.164	0.070	CHALFANT_A-SHE009	0.163	0.070	0.15	6.49
							CHALFANT_A-SHE099	0.091	0.055	0.19	5.19
20	CHICHI03_CHY024	0.207	0.359	1.72	0.187	0.334	CHICHI03_CHY024-E	0.187	0.331	0.71	1.41
							CHICHI03_CHY024-N	0.089	0.140	0.49	2.02
22	CHICHI03_TCU075	0.271	0.270	3.51	0.252	0.260	CHICHI03_TCU075-E	0.224	0.249	0.34	2.95
							CHICHI03_TCU075-N	0.153	0.105	0.25	4.07
24	CHICHI03_TCU122	0.263	0.346	2.79	0.212	0.301	CHICHI03_TCU122-E	0.201	0.299	0.61	1.65
							CHICHI03_TCU122-N	0.170	0.175	0.25	3.93
29	CHICHI04_CHY080	0.178	0.227	2.89	0.132	0.180	CHICHI04_CHY080-E	0.132	0.146	0.33	3.06
							CHICHI04_CHY080-N	0.120	0.174	0.37	2.73
31	ITALY_B-CTR	0.242	0.345	2.22	0.240	0.278	ITALY_B-CTR000	0.177	0.232	0.48	2.10
							ITALY_B-CTR270	0.165	0.256	0.43	2.34
32	ITALY_B-VLT	0.138	0.152	3.36	0.111	0.140	ITALY_B-VLT000	0.099	0.127	0.33	3.01
							ITALY_B-VLT270	0.096	0.084	0.27	3.71
35	PALMSPR_CAB	0.304	0.180	6.74	0.232	0.180	PALMSPR_CAB180	0.217	0.076	0.14	7.21
							PALMSPR_CAB270	0.213	0.163	0.16	6.28

**Table 1** continued

Earthquake characteristics											
#	Earthquake record	PGA (SRSS <sup>a</sup> ) (g)	PGV (SRSS) (m/s)	Mean Frequency f <sub>m</sub> (Hz)	PGA (RES <sup>b</sup> ) (g)	PGV (RES) (m/s)	Horizontal components	PGA (g)	PGV (m/s)	Mean Period T <sub>m</sub> (s)	Frequency f <sub>m</sub> (Hz)
0.25 g < PGA < 0.5 g											
37	CHALFANT_A-ZAK	0.600	0.578	3.70	0.448	0.472	CHALFANT_A-ZAK270	0.447	0.369	0.24	4.14
							CHALFANT_A-ZAK360	0.400	0.445	0.31	3.25
38	CHICHIO3_CHY080	0.521	0.744	2.13	0.475	0.700	CHICHIO3_CHY080-E	0.473	0.699	0.52	1.94
							CHICHIO3_CHY080-N	0.218	0.255	0.43	2.33
39	CHICHIO3_TCU071	0.427	0.185	8.40	0.391	0.141	CHICHIO3_TCU071-E	0.194	0.132	0.14	7.10
							CHICHIO3_TCU071-N	0.380	0.130	0.10	9.70
40	CHICHIO3_TCU076	0.547	0.624	3.31	0.530	0.623	CHICHIO3_TCU076-E	0.524	0.593	0.35	2.82
							CHICHIO3_TCU076-N	0.156	0.195	0.26	3.81
41	CHICHIO4_CHY074	0.474	0.499	3.18	0.368	0.423	CHICHIO4_CHY074-E	0.323	0.322	0.34	2.93
							CHICHIO4_CHY074-N	0.347	0.381	0.29	3.43
42	CHICHIO6_TCU078	0.462	0.445	4.43	0.357	0.343	CHICHIO6_TCU078-E	0.254	0.284	0.26	3.84
							CHICHIO6_TCU078-N	0.386	0.343	0.20	5.01
43	FRIULI_A-TMZ	0.472	0.379	4.39	0.389	0.310	FRIULI_A-TMZ000	0.351	0.220	0.20	4.91
							FRIULI_A-TMZ270	0.315	0.308	0.26	3.87
44	MAMMOTH_J-LUL	0.508	0.273	5.21	0.460	0.247	MAMMOTH_J-LUL000	0.430	0.236	0.18	5.62
							MAMMOTH_J-LUL090	0.271	0.139	0.21	4.79
45	MAMMOTH_J-MLS	0.400	0.213	7.79	0.383	0.179	MAMMOTH_J-MLS254	0.321	0.157	0.13	7.72
							MAMMOTH_J-MLS344	0.239	0.143	0.13	7.87
46	MORGAN_AND	0.512	0.374	4.07	0.459	0.330	MORGAN_AND250	0.423	0.253	0.22	4.61
							MORGAN_AND340	0.289	0.276	0.28	3.54
47	NWCHINA3_J411	0.406	0.402	4.38	0.411	0.370	NWCHINA3_J411N000	0.300	0.193	0.19	5.20
							NWCHINA3_J411N270	0.274	0.353	0.28	3.56



**Table 1** continued

Earthquake characteristics											
#	Earthquake record	PGA (SRSS <sup>a</sup> ) (g)	PGV (SRSS) (m/s)	Mean Frequency f <sub>m</sub> (Hz)	PGA (RES <sup>b</sup> ) (g)	PGV (RES) (m/s)	Horizontal components	PGA (g)	PGV (m/s)	Mean Period T <sub>m</sub> (s)	Frequency f <sub>m</sub> (Hz)
PGA < 0.5 g											
48	BIGBEAR_BLC	0.727	0.445	7.03	0.646	0.350	BIGBEAR_BLC270	0.481	0.282	0.14	7.27
							BIGBEAR_BLC360	0.545	0.345	0.15	6.79
49	CHICHI03_TCU129	1.030	0.421	6.47	0.976	0.399	CHICHI03_TCU129-N	0.396	0.397	0.13	7.98
							CHICHI03_TCU129-E	0.951	0.141	0.20	4.96
50	CHICHI06_TCU079	0.993	0.591	5.98	0.775	0.507	CHICHI06_TCU079-N	0.622	0.502	0.15	6.68
							CHICHI06_TCU079-E	0.774	0.312	0.19	5.29
51	CHICHI06_TCU080	0.713	0.457	8.26	0.646	0.414	CHICHI06_TCU080-E	0.469	0.286	0.13	7.47
							CHICHI06_TCU080-N	0.538	0.357	0.11	9.06
52	COALINGA_H-PVY	0.808	0.703	4.34	0.599	0.602	COALINGA_H-PVY045	0.592	0.602	0.28	3.61
							COALINGA_H-PVY135	0.551	0.363	0.20	5.08
53	MORGAN_CYC	1.480	0.959	4.89	1.310	0.818	MORGAN_CYC195	0.711	0.516	0.21	4.69
							MORGAN_CYC285	1.298	0.808	0.20	5.08
54	PALMSPR_NPS	0.914	0.806	4.54	0.613	0.739	PALMSPR_NPS210	0.594	0.732	0.31	3.21
							PALMSPR_NPS300	0.694	0.338	0.17	5.87
55	VICT_CPE	0.855	0.373	4.22	0.639	0.319	VICT_CPE045	0.621	0.316	0.26	3.78
							VICT_CPE315	0.587	0.199	0.21	4.66

**Table 1** continued

Dynamic excitation response					
#	Earthquake record	Non-joined (cylindrical)		Joined (rectangular)	
		Top displacement $\delta$ (%) <sup>c</sup>	Post-seismic condition <sup>d</sup>	Top displacement $\delta$ (%)	Post-seismic condition
0.10 g < PGA < 0.25 g					
0	THESS_CITY78	6.2	SP	0.0	N
19	CHALFANT_A-SHE	2.7	N	0.0	N
20	CHICHI03_CHY024	>100	C	0.0	N
22	CHICHI03_TCU075	23.2	SP	0.0	N
24	CHICHI03_TCU122	63.7	N	0.0	N
29	CHICHI04_CHY080	20.4	SP	0.0	N
31	ITALY_B-CTR	72.8	SP	0.0	N
32	ITALY_B-VLT	34.8	SP	0.0	N
35	PALMSPR_CAB	12.0	SP	0.0	N
0.25 g < PGA < 0.5 g					
37	CHALFANT_A-ZAK	32.5	SP	35.2	HP
38	CHICHI03_CHY080	>100	C	17.4	N
39	CHICHI03_TCU071	7.5	SP	2.2	N
40	CHICHI03_TCU076	29.3	N	13.5	N
41	CHICHI04_CHY074	>100	C	0.0	N
42	CHICHI06_TCU078	46.8	SP	0.1	N
43	FRIULI_A-TMZ	26.1	SP	0.0	N
44	MAMMOTH_I-LUL	19.2	SP	0.0	N
45	MAMMOTH_I-MLS	14.8	SP	0.0	N
46	MORGAN_AND	34.1	SP	0.7	N
47	NWCHINA3_J411	41.9	SP	0.0	N

**Table 1** continued

Dynamic excitation response					
#	Earthquake record	Non-joined (cylindrical)		Joined (rectangular)	
		Top displacement $\delta$ (%) <sup>c</sup>		Top displacement $\delta$ (%)	
		Post-seismic condition <sup>d</sup>		Post-seismic condition	
PGA < 0.5 g					
48	BIGBEAR_BLC	19.8	N	14.5	HP
49	CHICHI03_TCU129	77.2	SP	9.1	N
50	CHICHI06_TCU079	21.9	SP	61.8	HP
51	CHICHI06_TCU080	46.4	HP	6.2	N
52	COALINGA_H-PVY	40.0	HP	52.1	HP
53	MORGAN_CYC	48.6	HP	58.8	HP
54	PALMSPR_NPS	63.6	HP	24.3	SP
55	VICT_CPE	24.4	SP	45.3	N

<sup>a</sup> SRSS square root of the sum of squares of the horizontal seismic components<sup>b</sup> RES maximum amplitude of the resultant vector of the horizontal seismic components<sup>c</sup>  $\delta$  displacement of the highest point of the shaft over the displacement capacity [%]<sup>d</sup> N no permanent rotation or dislocation, SP permanent slight rotation or dislocation, HP permanent high rotation or dislocation, C collapse

et al. 2011). Both the normal and shear joint stiffness were set to  $5 \times 10^8$  kPa/m. The seismic motion was imposed as velocity time-histories at the rigid sub-base of the structure (Fig. 2). The damping of the system was taken as Rayleigh stiffness-proportional with the damping constant  $\beta = 0.000083$  set to give critical damping for the surface impact frequency (DeJong 2009). Although this damping approach significantly increases the computational time cost and limits the number of analyses, it was deliberately adopted to obtain more realistic and robust numerical results.

It is noted that it is yet unclear whether the rectangular base of the column, i.e., block 2 in Fig. 2, was indeed connected with the shaft during the anastilosis (re-positioning) of 1969. This poses an important boundary condition issue, as if this is indeed the case, the oscillation of the column, on a rectangular base of 1.0 m, would be much different than that of a cylindrical column of a diameter 0.66 m without a connected base. The problem becomes more complex as it cannot be assessed a priori which configuration would lead to a more favourable seismic performance of the structure. While the connected column has a wider base and appears to be more resistant to overturning, no prediction can be really made regarding the resulting permanent deformations. Moreover, the tensile stress level that the connection can bear without sustaining any damage is also not known. Such a failure could be limited in the connection itself, i.e. failure of the bars (which is rather reversible), marble-mortar interface (also reversible) or marble-mortar matrix which is effectively irreversible damage (Marinelli et al. 2009). In a worst case scenario, it can also cause extended and irreversible damage to marble portions adjacent to the connection due to high stress concentrations. For all the above reasons dynamic analyses were comparatively performed for both configurations. Regarding the connected base-shaft in particular, blocks 2 and 3 were joined. In this joint, no slip, rotation or detachment was possible. For simplicity, the problem of the stress concentration was not investigated in this study.

The numerical results are presented in two forms. The first is the maximum displacement of the capital during the earthquake shaking. The second is the observation of a specific limit state, such as collapse or permanent deformation, expressed by relative displacement or rotation, after the end of the excitation.

The post-seismic condition is therefore divided in “no”, “slight” and “high” permanent deformations (Table 2). The assumption of the deformation limits was based on the displacements and rotations that can be easily perceived by naked eye. High permanent deformation is regarded as residual dislocation of the centre of the column base higher than 0.01 m or rotation that exceeds  $2.5^\circ$  (i.e., approximately 0.03 m of arc length for a cylindrical section). Slight permanent deformation is defined as exceeding the 10 % of the high deformation criterion. Those slight deformations cannot be identified with certainty on-site. However, their accumulation due to multiple seismic events can eventually produce visible deformations.

**Table 2** Permanent deformation limits

Post-seismic condition criteria	Rotation	Displacement of centre
No permanent deformation	$r < 0.25^\circ$	$d < 0.001$ m
Slight permanent deformation	$0.25^\circ \leq r < 2.5^\circ$	$0.001 \text{ m} \leq d < 0.01 \text{ m}$
High permanent deformation	$2.5^\circ \leq r$	$0.01 \text{ m} \leq d$

The displacement at the column top is expressed as the maximum calculated horizontal displacement during the oscillation normalised to the displacement capacity and is expressed as a percentage ratio. The displacement capacity was approximated as 0.66 and 1.00 m for the non-joined and joined configurations, respectively. Displacement capacity is defined as the minimum level of horizontal displacement for which the loss of equilibrium of the rigid body results to overturning. For the non-joined configuration this corresponds to the column diameter whereas for the joined element the displacement capacity is equal to the base width. It is worth noting though that those displacement limits can be slightly exceeded during the dynamic excitation without necessary overturning, if the restoring moment about the pole of rotation is able to restore the body back to equilibrium (Psycharis et al. 2013).

### 3.3 Ishiyama overturning criteria

Based on numerous shaking table tests and numerical simulations with harmonic and seismic excitations, Ishiyama (1984) managed to validate existing rocking mathematical expressions to propose new formulations and criteria for overturning of rigid bodies. According to his work, the behaviour of rigid bodies can be defined by their height and slenderness in combination with the amplitudes of the excitation maximum acceleration ( $\alpha_0$ ) and velocity ( $v_0$ ). These criteria were derived from sinusoidal excitations but were also valid for seismic excitation analyses. As shown in Fig. 3, neither rocking nor overturning can occur in region A, rocking can take place without overturning in region B and in C, overturning is probable.

The acceleration line is the boundary between areas A and B and defines the lower limit of maximum horizontal acceleration necessary for initiating rocking. This acceleration can also be found from the linear kinematic analysis. As rocking behaviour does not necessarily mean overturning probability, Ishiyama (1984) proposed a criterion for the lower limit of  $v_0$  that can result in overturning. Moreover, limit period ( $T_c$ ) was proposed indicating that in case that the input acceleration period is lower than  $T_c$ , then the acceleration must be much larger than the lower limit  $\alpha_0$  in order to overturn the body.

Furthermore, this study showed that the surface and edge static coefficients of friction, surface and edge kinetic coefficients and the tangent and normal restitution coefficients

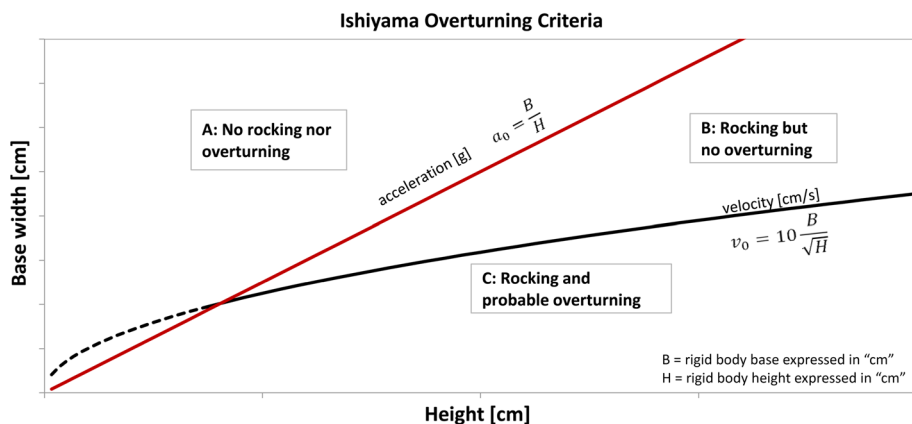


**Fig. 3** Ishiyama overturning criteria for rectangular rigid bodies

have a very small effect. Also, bigger bodies in region C had lower overturning probability than smaller ones with the same H/B ratio, thus validating the “size effect” theory described by Housner (1963).

For the studied column of the Roman Agora the slenderness of the non-joined and joined configuration is different, thus the minimum acceleration for the rocking initiation and minimum velocity for probable overturning also differ. The Ishiyama acceleration and velocity criteria for both cases are presented in Fig. 4.

## 4 Numerical analysis

### 4.1 Structural behaviour

The minimum acceleration demand for initiating rocking movement is calculated using linear kinematic analysis. With the rotation pole as the edge of the cylindrical base, the acceleration is around 0.10 g for the non-joined element. For the joined configuration, the minimum acceleration can vary between 0.15 and 0.21 g. This variance depends on the direction of the excitation. The lowest value corresponds to an idealized single-component excitation parallel to one edge of the base and a perfect 2D response. Although the DEM 3D response differs substantially from the simplified kinematic analysis, the minimum acceleration thresholds of uplift are still valid. Pure sliding would occur, with  $\mu = 0.7$ , only for an acceleration higher than 0.7 g, that is, a much higher value than the minimum acceleration for rocking initiation. This means that the predominant structural response to the selected accelerograms will be rocking oscillation. For the non-joined configuration, rocking was indeed observed for all completed analyses. However, for the joined configuration some analyses resulted to really low levels of oscillation although the accelerograms had a PGA higher than the minimum demands described before.

This can be easily explained by the frequency content of the high acceleration pulses. Lower frequencies result to higher exposure times to acceleration levels that can cause rocking and thus to higher energy input for the oscillating system. A comparison between accelerograms of similar PGA but different frequency content is shown in Fig. 5. It is clear that the #38 event (red thick line, also refer to Table 1) with lower frequent content than event #44 (blue thin line) inputs more energy and causes higher oscillation levels. In the

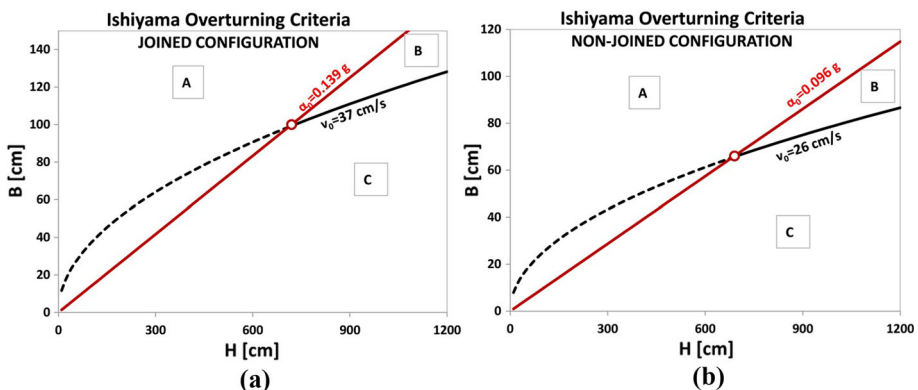


**Fig. 4** Acceleration and velocity criteria of Ishiyama for **a** non-joined and **b** joined configuration

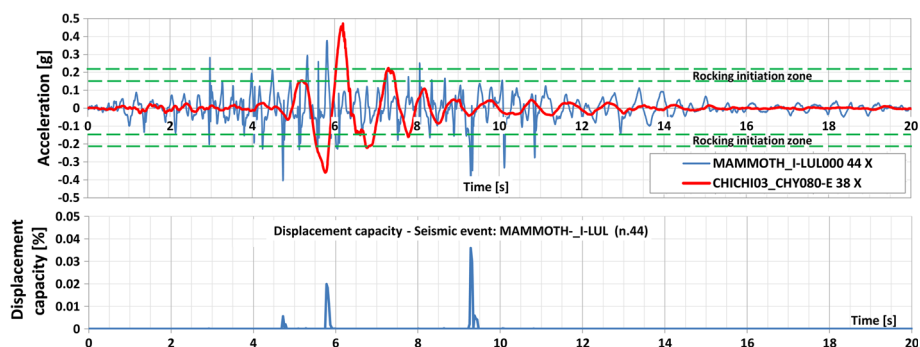


**Fig. 5** Comparison between accelerograms of similar PGA but different frequency content (*top*); top displacement of joined column configuration for seismic event #44 when PGA exceeded the rocking initiation levels (*bottom*)

same figure, the correlation between accelerogram #44× and uplift caused to the joined column configuration is presented. While the moments of uplift, i.e. when relative displacement of the top becomes positive, coincide with the surpassing of PGA rocking initiation limits, those strong pulses have a small duration and are quickly damped out without being able to produce a continuously rocking behaviour.

The structural response of the elements to the multi-directional seismic excitation depended strongly on the type of symmetry of their base. The joined configuration with square base usually either resulted into an oscillation parallel to, or not completely parallel but strongly influenced by, one of the two main axes. We observed that, as anticipated, the more oriented a motion was with an axis, the lower the permanent rotation value. The relative displacement between the base and capital (control point 17/21 in Fig. 2) is presented for analyses #53, #54 and #55 in Fig. 6. For seismic event #53 the main oscillation took place along the Y-axis but there was also a strong motion along the X-axis and a very high level of visible permanent rotation at around  $27^\circ$ . In contrast, the analysis of #54 had a very low level of motion along the weak axis and a slight permanent rotation around  $0.9^\circ$ . The analysis of the #55 seismic event manifested the highest level of motion but this was completely parallel with the axis X. Naturally, this analysis yielded almost zero levels of permanent rotation ( $0.01^\circ$ ) and dislocation of the centre (0.2 mm). In the depicted graphs, the red dashed line represents the maximum capacity of top displacement, which, if exceeded, results in an overturning of the column. A typical example of the deformed shape of the joined configuration with a final rotation of  $7^\circ$  for the earthquake #50 is

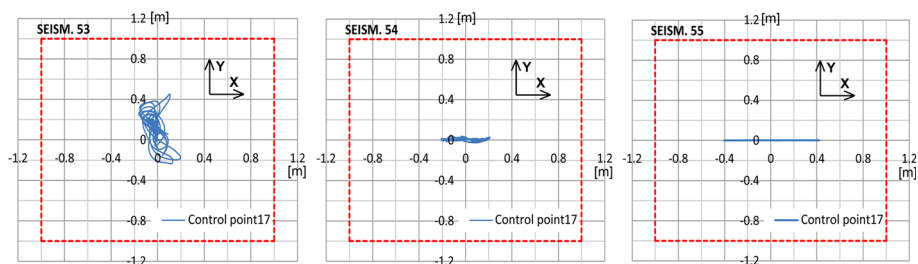


**Fig. 6** Relative displacement of control point 17 of the capital for joined configuration: structural response weakly (*left*) strongly (*centre*) and absolutely (*right*) influenced by a main axis of symmetry

presented in Fig. 7. Moreover, although the capital was not linked to the shaft, neither collapse of the capital nor substantial relative displacements between the capital and shaft was observed.

The non-joined element on the other hand, exhibited a different behaviour. Due to its circular base section and its axisymmetric nature, the non-joined configuration is free to oscillate following the direction of the imposed excitation. The most usual way of oscillation is wobbling around the circular perimeter as presented in the graphs of the displacement on the top for earthquakes #53, #54 and #55 (Fig. 8). The residual deformation in terms of rotation is accumulated during this wobbling motion and depends on the amplitude and duration of the oscillation.

A comparison of the graphs of Fig. 8 with those of Fig. 6 for the same seismic events underlines the difference of structural response between non-joined and joined configurations.

An interesting observation is, however, that the non-joined element may also exhibit a rocking oscillation along the strongest component direction. For instance, one of the two horizontal components of seismic event #49 (Fig. 9a) had a significantly higher PGA and PGV causing rocking along one main direction. However, the rocking oscillation can also appear continuously rotating direction as in the case of earthquake #42 (Fig. 9b). Figure 9c, shows one of the three analyses where collapse occurred when the maximum displacement capacity (red dashed line) was exceeded. The fact that the analyses that yielded mainly rocking and low wobbling motions tended to have low levels of residual rotation suggests that permanent deformation of this type is mainly produced during wobbling motion.

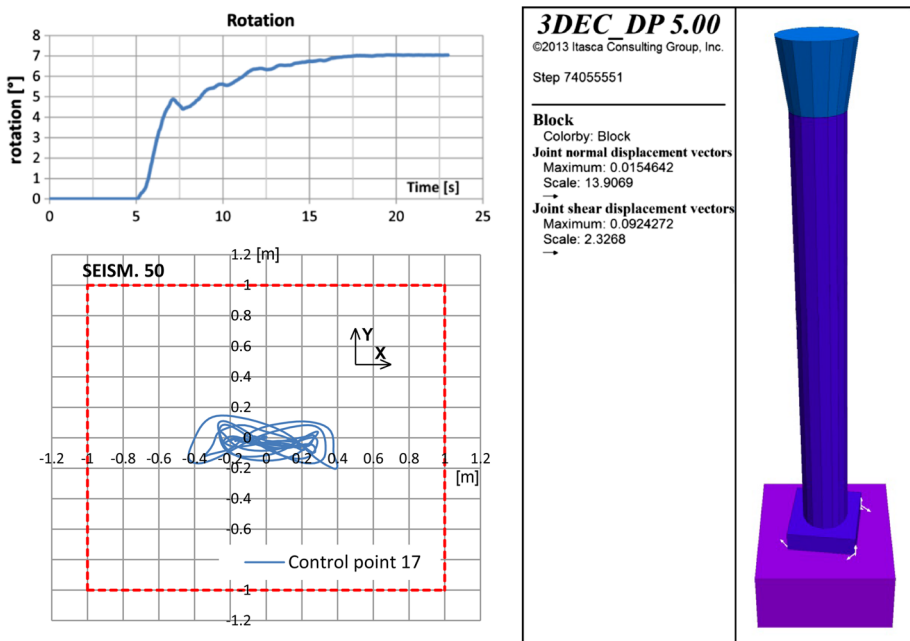


**Fig. 7** Rotation time-history (*top*); displacement of control point 17 of the capital (*bottom*) and deformed shape (*right*) of joined configuration for earthquake #50



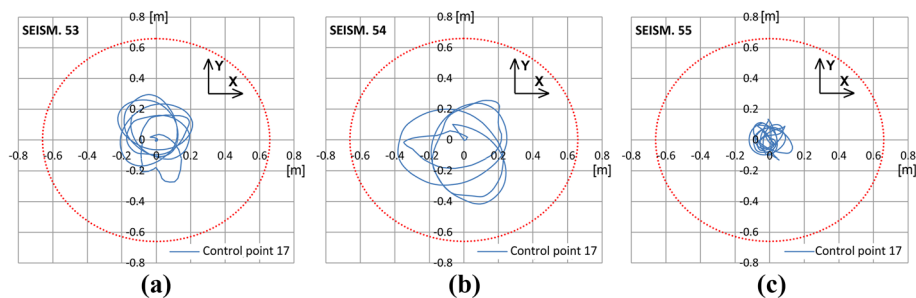


**Fig. 8** Relative displacement of the control point 17 of the capital for non-joined configuration performing wobbling oscillation

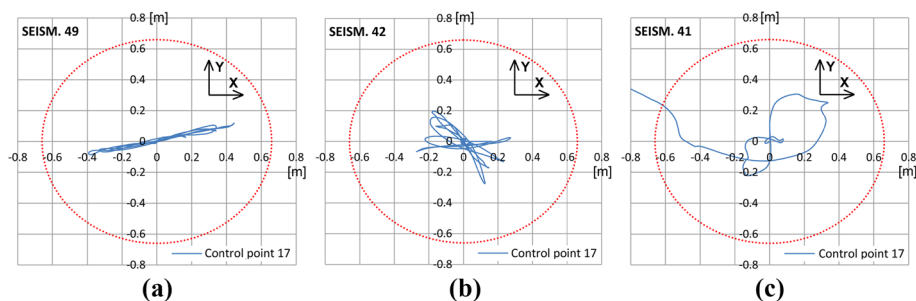


**Fig. 9** Relative displacement of the control point 17 of the capital for non-joined configuration. **a** Rocking along one direction; **b** rocking along a rotating direction; **c** overturning

## 4.2 Maximum displacement

A correlation analysis was performed between the numerical outputs, i.e. the maximum reached level of displacement capacity ( $\delta$ ), and the analysis inputs in terms of PGA and PGV. This was done for assessing the efficiency of both earthquake intensity measures to predict the structural response of rocking structures. The correlation analysis has been possible using two different dimensionless indicators. Both can take values between zero and one, indicating a weak or strong correlation between the variables, respectively. The first indicator is the correlation coefficient  $r_{xy}$  that measures the strength of linear relationship between a given pair of variables. The second indicator of correlation is the determination coefficient  $R^2$  defined as the ratio of the variances of the fitted values of the used model and the measured values of the dependent variable. Here, a linear regression model was used.

In all cases,  $\delta$  is the dependent variable. The independent variables are PGA and PGV taken both as the amplitude of Square Root of the Sum of Squares (SRSS) of the two horizontal components and as maximum amplitude of the resultant (RES) vector of the two components. For the correlation and determination coefficient calculation, the three analyses that resulted in the collapse of the non-joined configuration were not considered due to the fact that no specific maximum displacement can be defined for overturning bodies.

As shown in Figs. 10, 11, 12, 13 and Table 3, all coefficients of correlation and determination are low. This signifies that it is not possible to achieve a good fit between the intensity measure and the response variables, which enables an accurate prediction of the

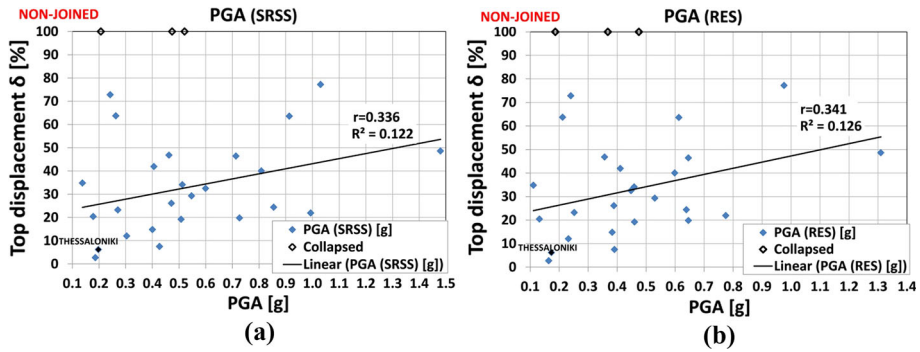


**Fig. 10** Dispersion graphs of the independent variables  $PGA_{(SRSS)}$  and  $PGA_{(RES)}$  and the dependent variable  $\delta$  for the non-joined configuration

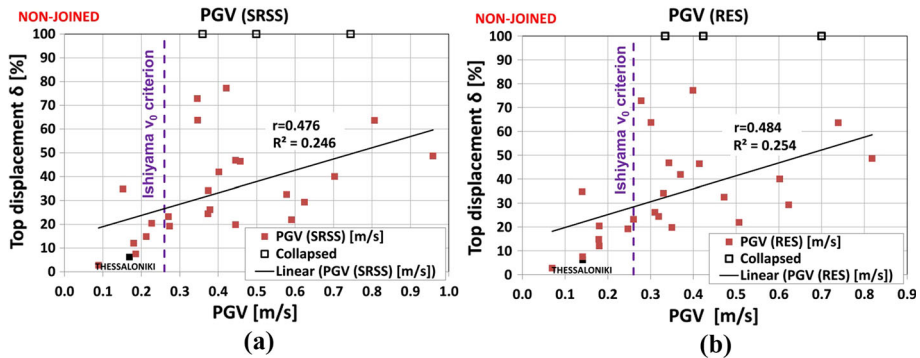


**Fig. 11** Dispersion graphs of the independent variables  $PGV_{(SRSS)}$  and  $PGV_{(RES)}$  and the dependent variable  $\delta$  for the non-joined configuration

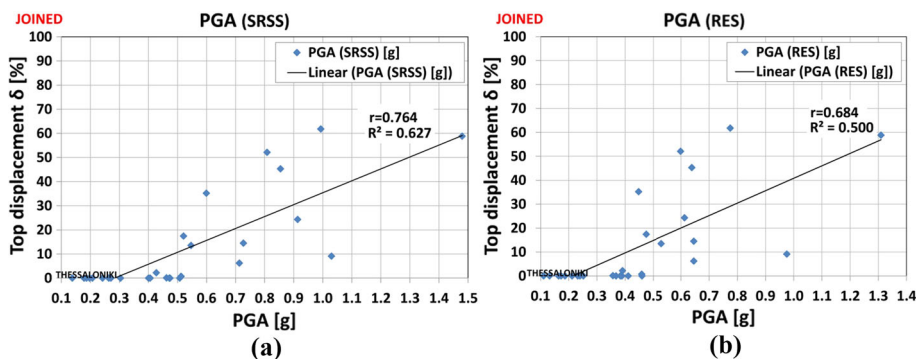


**Fig. 12** Dispersion graphs of the independent variables  $PGA_{(SRSS)}$  and  $PGA_{(RES)}$  and the dependent variable  $\delta$  for the joined configuration

structural response  $\delta$  using only the independent input variables. This also explains why it is necessary to follow a probabilistic approach for such a multi-parametric problem, as early proposed by Yim et al. (1980).

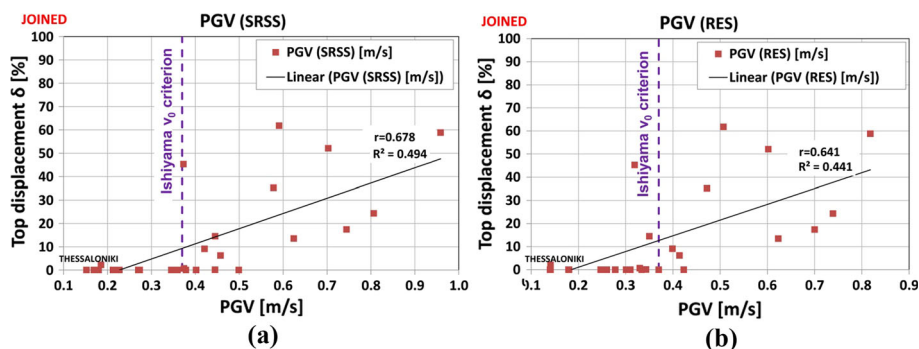


**Fig. 13** Dispersion graphs of the independent variables  $PGV_{(SRSS)}$  and  $PGV_{(RES)}$  and the dependent variable  $\delta$  for the joined configuration

**Table 3** Correlation and determination coefficients for  $\delta$ -PGA and  $\delta$ -PGV pairs of variables

	Correlation Coefficient $r_{x,y}$				Determination coefficient $R^2$			
	Non-joined		Joined		Non-joined		Joined	
	PGA	PGV	PGA	PGV	PGA	PGV	PGA	PGV
(SRSS)	0.336	0.476	0.764	0.678	0.122	0.246	0.627	0.494
(RES)	0.341	0.484	0.684	0.641	0.126	0.254	0.684	0.441

The comparison of the coefficients of correlation and determination for PGA and PGV shows interesting results. For the non-joined configuration the correlation between the pair  $\delta$ -PGV is stronger than that of  $\delta$ -PGA (Figs. 10, 11). However, this is completely reversed for the joined column where the  $\delta$ -PGA pair is more correlated (Figs. 12, 13). For this configuration the  $\delta$ -PGA pair remains more correlated than the  $\delta$ -PGV even if the analyses with no rocking motion are not considered.

A comparison of the coefficients for the SRSS with those of the RES amplitudes did not yield any significant difference. The RES amplitudes were marginally more correlated than SRSS for the non-joined configuration (Figs. 10, 11). A more notable correlation was observed for the SRSS of the joined configuration for both the  $\delta$ -PGA and  $\delta$ -PGV (Figs. 12, 13) pairs. As a result of these findings, the data presented is a function of SRSS and not RES amplitudes.

Moreover, the influence of the earthquake frequency content to the maximum levels of rocking oscillation was studied. To do so, the effect of the mean frequency  $f_m = 1/T_m$  on the structural response was examined by observing the levels of  $\delta$  for the various  $f_m$ -PGA and  $f_m$ -PGV combinations. Regarding the non-joined configuration, the results shown in Fig. 14, indicate that the  $f_m$  influence is strong. If the presented frequency axis is divided in two equal parts, i.e. 1.5–5.0 Hz and 5.0–8.5 Hz, it is clear that the analyses with higher levels of  $\delta$  are mainly concentrated in the low frequency area. This can be seen in both  $f_m$ -PGA and  $f_m$ -PGV graphs. Moreover, the three analyses for which the column collapsed correspond to low mean frequencies of 2.13 and 3.18 Hz. However, the simultaneous influence of the independent variable in combination with  $f_m$  is more evident in the case of

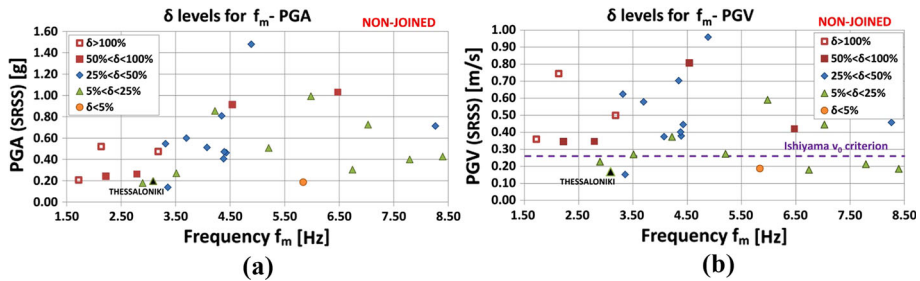


**Fig. 14**  $\delta$  levels for pairs of  $f_m$ -PGA (a) and  $f_m$ -PGV (b) for non-joined configuration

PGV than PGA. In Fig. 14b it is shown that in addition to the subdivision in low and high frequency domains,  $\delta$  also increases with the increase of the PGV amplitude.

Furthermore, the applicability of the Ishiyama criterion for the PGV was examined. The results yielded strong correlation between the Ishiyama criterion and the maximum horizontal displacement during rocking. For the non-joined element, no records with a  $\delta$  value higher than 25 % were reported under the Ishiyama line (Fig. 14b), while the levels of  $\delta$  increase drastically for PGV values just over this criterion. Using the  $f_m$ -PGV graph, it is possible to propose three different risk zones regarding the combination of  $f_m$ -PGV. The high risk zone is where all three analyses yielded collapse and most of the analyses with  $\delta$  higher than 50 % are concentrated. This is defined by a PGV higher than 0.26 m/s, which is the Ishiyama criterion and frequencies up to around 3.5 Hz. The intermediate zone that concentrates most of the analyses with  $\delta$  between 25 and 50 % has the same PGV lower limit and frequencies ranging from 3.5 Hz to 6.5 Hz. The rest is defined as the low risk zone.

As expected, the joined-element manifested a more stable behaviour with no analyses indicating collapse. As shown in Fig. 15, there is a large zone within which no or little rocking occurs with a  $\delta$ -value lower than 5 %. This zone is well defined for the  $f_m$ -PGA with a limit acceleration of around 0.50 g. Also note, that there is no analysis with a  $\delta$  value higher than 5 % for levels of PGV lower than the Ishiyama velocity criterion. Most of the low  $f_m$  excitations that had low PGA and PGV amplitudes resulted in low displacements. The highest  $\delta$  levels were recorded for the highest amplitudes of the PGA and PGV, i.e. higher than 0.81 g and 0.59 m/s respectively, which corresponded to excitation of a medium level  $f_m$  between 3.5 and 6.5 Hz.

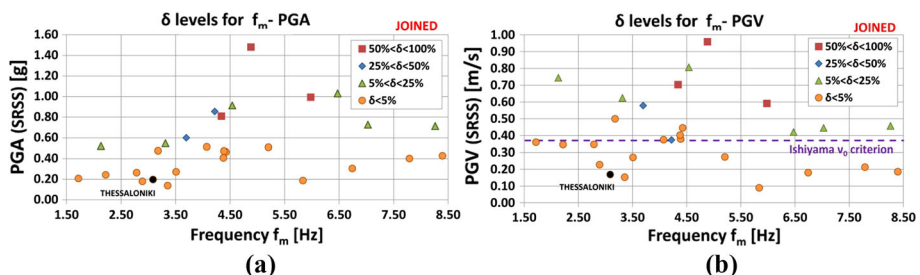


**Fig. 15**  $\delta$  levels for pairs of  $f_m$ -PGA (a) and  $f_m$ -PGV (b) for joined configuration

### 4.3 Post-seismic condition

An additional aim of this work was to investigate the correlation between the post-seismic permanent deformations and the PGA, PGV and  $f_m$  values. This is important for examining if back-analysis, estimating the earthquake IM values of past seismic events, based on the deformation patterns and amplitudes manifested in ancient free-standing columns is possible. The level of permanent deformations was measured after the end of each analysis. The post-seismic condition results are shown in Table 2 and more detailed in Tables 4 and 5. Note that all analyses with deformed elements manifested mainly rotational deformations and not direct sliding towards one direction. In addition, intense rocking oscillation and residual deformations were not strictly correlated. Analyses with high  $\delta$  values indicated a return to rest position with no visible deformations while others with much lower  $\delta$  levels were found rotated with respect to their initial position. For instance, analyses #24, #31 and #49 of the non-joined configuration reached  $\delta$  levels between 63.7 and 77.2 % but manifested only slight or no post-seismic permanent deformations. No clear boundaries were found between non-deformed and deformed condition considering the PGA and PGV amplitudes independently. Instead, an upper bound for the non-deformed condition can be set considering combinations of PGA and PGV values.

For the non-joined configuration, permanent deformations were recorded for the whole range of tested PGA and PGV amplitudes. If collapsed analyses were not considered, the tests with high permanent deformations were those with a PGA higher than 0.71 g and a PGV higher than 0.46 m/s (Fig. 16). However, the zone under those limits appears both non-deformed and slightly deformed elements, preventing the definition of a clear boundary between them. Although the statistical sample is small, analyses with the combination of PGA and PGV higher than 0.71 g and 0.46 m/s all caused slight or high permanent deformations. This can be set as an estimation for the upper bound, which if exceeded predicts a slight or high permanent deformation for the cylindrical column.

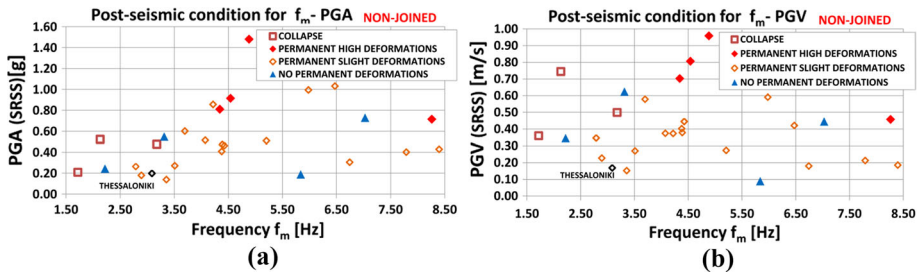
For the joined configuration, less analyses lead to permanent deformations but when this happened it usually concerned high deformations. As expected, the analyses with very low levels or no rocking did not cause any deformations. Similar to the non-joined case, the analyses with deformed post-seismic condition cover a wide range of PGA and PGV values. For the analyses where  $\delta$  was higher than 5, 55 % (six out of eleven tests) presented

**Table 4** Values of post-seismic rotation and dislocation for the non-joined element

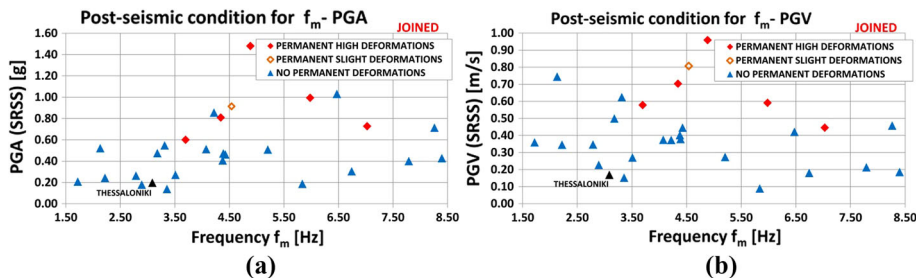
Non-joined configuration: rotation (°)/dislocation of centre (mm)						
#0	#19	#20	#22	#24	#29	#31
0.61/0	0.2/0	Collapsed	0.29/0	0.19/1	0.46/0	0.2/3
#32	#35	#37	#38	#39	#40	#41
2.06/3	1.05/1	2.05/3	Collapsed	0.77/0	0/0	Collapsed
#42	#43	#44	#45	#46	#47	#48
0.20/1	0.31/2	2.49/1	0.82/1	1.42/1	2.3/2	0.1/0
#49	#50	#51	#52	#53	#54	#55
0.62/1	1.67/2	4.8/2	2.50/2	10.0/5	8.9/6	1.5/1

**Table 5** Values of post-seismic rotation and dislocation for the joined element

Joined configuration: rotation (°)/dislocation of centre (mm)						
#0	#19	#20	#22	#24	#29	#31
0/0	0/0	0/0	0/0	0/0	0/0	0/0
#32	#35	#37	#38	#39	#40	#41
0/0	0/0	8.9/2	0/0	0/0	0/0	0/0
#42	#43	#44	#45	#46	#47	#48
0/0	0/0	0/0	0/0	0/0	0/0	3.49
#49	#50	#51	#52	#53	#54	#55
0.06/0	7.0/0	0.16/0	16.5/1	28.8/5	0.93/1	0.02/0

**Fig. 16** Post-seismic condition for pairs of  $f_m$ -PGA (a) and  $f_m$ -PGV (b) for non-joined configuration

permanent deformations. Unlike the non-joined element, there was no zone with no deformations and slight deformations results. Instead, the joined element had a tendency to either remain undeformed or to appear highly rotated. As presented in Fig. 17, five out of the six deformed analyses appear high and only one yielded slight deformation. Here it is easier to set a minimum level of PGA and PGV values under which no deformation takes place. This level coincides with the amplitude of PGA and PGV under which no rocking oscillation takes places. The PGV limit is set close to the Ishiyama velocity criterion while the lowest PGA that caused rocking and thus probable deformation, was around 0.5 g. Note that all analyses that combined a PGA higher than 0.61 g and a PGV higher than 0.46 m/s led to permanent deformations. This combination can be set as the upper bound for the non-deformed condition.

**Fig. 17** Post-seismic condition for pairs of  $f_m$ -PGA (a) and  $f_m$ -PGV (b) for joined configuration

## 5 Seismic performance: 1978 Thessaloniki earthquake and Greek Seismic Code

As already presented, the correlation indicators for both PGA and PGV and the structural response are rather low, when examined individually. This explains the need to consider both IM simultaneously, along with the mean frequency of the seismic motion  $f_m$ , for a complete vulnerability assessment. Based on these findings, a back-analysis was performed for assessing the seismic performance of the column during the 1978 Thessaloniki earthquake, in which the column resisted without sustaining any visible permanent deformations.

The numerical analyses of the main shock of 20/06/1978 scenario were carried out both for the joined and non-joined column and base configuration. The three components of the ground motion recorded at a distance of 900 m were used as input. The results of the analysis confirm the column's ability to resist the 1978 event with either non-joined or joined configurations. For the non-joined element, the SRSS amplitude of the PGA that resulted in collapse was 0.207 g, very close to the 0.197 g value of the 1978 main shock. Moreover, two records with a low PGA, i.e. 0.24 g and 0.26 g, and an  $f_m$  close to the examined resulted in very high  $\delta$  levels of around 73 and 64 % respectively (Fig. 14a). Although from this finding it may seem that the 1978 earthquake could have been hazardous for the non-joined column, the real situation is clarified by examining the  $f_m$ -PGV graph in Fig. 14b. In this graph, the PGV level is much lower than the limit PGV value (0.26 m/s) for collapse or high top displacements. Moreover, the PGV amplitude of 1978 was even lower than the Ishiyama velocity criterion which defines the zone of overturning probability. Since the joined configuration the PGA and PGV are not even close to the area where rocking initiates, it is expected that the risk of collapse was even lower. Together, these data verify that the 1978 main shock did not jeopardize the stability of the column and did not cause high displacements near the collapse threshold.

The consideration PGV was also necessary for the seismic vulnerability assessment which was carried out for the 475 years of recurrence earthquake as foreseen by the Greek Seismic Code. According to Leventakis (2003), for loose soil conditions the expected PGA and PGV levels are 0.179 g and 0.15 m/s. For the more vulnerable non-joined configuration, the column capacity in terms of PGV, i.e. 0.26 m/s, exceeds by far the expected PGV level. Based on those findings and according to the current knowledge on the seismicity of Thessaloniki, the risk of collapse due to a probable earthquake event is assessed as low for the studied ancient column of the Roman Agora.

## 6 Conclusions

This work investigated the efficiency of using PGA and PGV as earthquake IM for the seismic vulnerability assessment of monolithic rocking bodies. To do so, a three-dimensional model of an existing free-standing ancient column was analysed with the DEM approach. A set of twenty-eight (28) specifically selected earthquake records was used for the non-linear response-history analyses. The IM efficiency assessment was based on the dispersion of the Engineering Demand Parameters, i.e., maximum displacement and permanent deformation. Note that it was not possible to calibrate the DEM model based on the Thessaloniki event because the earthquake intensity on the site of interest was not adequate to cause any displacements or rotations. As a result, the parameters used in the analytical

model (stiffness, friction, cohesion, damping) were based on bibliography. This does not reduce the interest of the study, which is essentially a sensitive analysis of the most important parameters controlling the response of free-standing columns. The principal conclusions drawn from this study can be summarized as follows:

1. The correlation of PGA and PGV with the numerical outputs is weak. This implies that the structural response cannot be predicted accurately based only on individual earthquake intensity proxies. For the non-joined column configuration, the PGV amplitude was found better correlated with the maximum displacements compared to PGA (i.e.  $r$  is equal to 0.476 for PGV versus 0.336 for PGA). The opposite was observed for the joined configuration where the correlation was higher for the PGA amplitude (i.e.  $r$  is equal to 0.678 for PGV versus 0.764 for PGA).
2. A strong influence of the mean frequency of the ground motions,  $f_m$ , on the structural response was observed. More precisely, for the non-joined column, high frequency motions with  $f_m$  between 1.5 and 3.5 Hz, in combination with a PGV higher than 0.26 m/s, tend to increase the level of horizontal displacement during rocking. For the joined configuration, the analyses with average levels of  $f_m$  (i.e. between 3.5 and 6.5 Hz) and high levels of PGA and PGV, i.e. 0.81 g and 0.59 m/s respectively, yielded the highest relative displacement of the top of the column. Along these lines, it is deemed more efficient to consider dual Intensity Measures such as, (PGA,  $f_m$ ) and (PGV,  $f_m$ ) pairs, instead of single PGA and PGV amplitudes.
3. High residual deformations are not necessarily evidence of strong rocking motion. In fact, no correlation was observed between the maximum displacements during shaking and the existence and level of post-seismic permanent deformations. Note the analyses #24, #31 and #49 which manifested very high levels of  $\delta$  but only slight or no permanent post-seismic deformations. It was proven difficult to set precise boundaries of the IM's beyond which permanent deformations are certain. However, it was observed that for the non-joined element, all analyses with a PGA higher than 0.70 g and a PGV higher than 0.46 m/s led to permanent deformations. Similarly, for the joined configuration, analyses with a PGA higher than 0.61 g and a PGV higher than 0.46 m/s caused permanent deformations.
4. The permanent deformations for the cylindrical base column were found to be mainly the result of wobbling motion. This can be shown by comparing the seismic response of the non-joined configurations for the seismic events #53 and #49. For seismic event #53, intense wobbling led to a very high level of permanent rotation at while for the #49 which performed strong oscillation but in one direction, no permanent deformations were manifested. Regarding the case of the joined-column with the rectangular base, permanent deformations were attributed to rocking oscillation deviated from one of the two axes of symmetry. This is shown better in the comparison of the analyses #53 and #55. For seismic event #53 the column performed strong oscillation took along two axes, a very high level of visible permanent rotation was registered. In contrast, for the #55 seismic which caused a strong oscillation but only along one axis, no permanent deformations were manifested.
5. The collapse probability of the examined Roman Agora column examined in the framework of the case study, was assessed as low for the level of ground motion foreseen by the Greek Seismic Code (and Eurocode 8) for conventional new structures. More specifically, the column capacity in terms of PGV, i.e. 0.26 m/s, is much higher than the corresponding Code value which is equal to 0.15 m/s. As anticipated, based



on the column PGV capacity, back analysis confirmed its stability during the 1978 earthquake when PGV did not exceed 0.17 m/s.

**Acknowledgements** The authors would like to thank Prof. R. Genevois of the Department of Geosciences of the University of Padova for the excellent collaboration and the permission to use the licence of the discrete element software for carrying out all necessary analyses. They also wish to thank Emeritus Professor of Aristotle University Thessaloniki, Kosmas Stylianidis for his valuable advice on various aspects throughout this study.

**Open Access** This article is distributed under the terms of the Creative Commons Attribution 4.0 International License (<http://creativecommons.org/licenses/by/4.0/>), which permits unrestricted use, distribution, and reproduction in any medium, provided you give appropriate credit to the original author(s) and the source, provide a link to the Creative Commons license, and indicate if changes were made.

## References

- Acikgoz MS, DeJong MJ (2012) Characterizing the vulnerability of flexible rocking structures to strong ground motions. In: 15th Word Conf Earthq Eng
- Adam-Veleni P (2001) The work in the Ancient Agora in Thessaloniki in the last ten years (in Greek). In: Proc. Conf. Work. years 1989–1999 Thessaloniki. pp 15–38, 323–326
- Ambraseys N, Douglas J, Rinaldis D et al (2004) Dissemination of European strong-motion data, CD-ROM collection. Eng Phys Sci Res Counc, UK
- Augusti G, Sinopoli A (1992) Modeling the dynamics of large block structures. *Meccanica* 17:195–211
- Baker JW (2011) The conditional mean spectrum: a tool for ground motion selection. *J Struct Eng* 137:322–331. doi:[10.1061/\(ASCE\)ST.1943-541X.0000215](https://doi.org/10.1061/(ASCE)ST.1943-541X.0000215)
- Baker JW, Cornell CA (2005) A vector-valued ground motion intensity measure consisting of spectral acceleration and epsilon. *Earthq Eng Struct Dyn* 34:1193–1217. doi:[10.1002/eqe.474](https://doi.org/10.1002/eqe.474)
- Bommer JJ, Acevedo AB (2004) The use of real earthquake accelerograms as input to dynamic analysis. *J Earthq Eng* 8:43–91. doi:[10.1080/13632460409350521](https://doi.org/10.1080/13632460409350521)
- Bommer J, Acevedo A, Douglas J (2003) The selection and scaling of real earthquake accelerograms for use in seismic design and assessment. In: Proc Int Conf Seism Bridg Des retrofit, Am Concr Inst
- Bray J, Rodriguez-Marek A (2004) Characterization of forward-directivity ground motions in the near-fault region. *Soil Dyn Earthq Eng* 24:815–828
- Cundall P (1976) Explicit finite difference methods in geomechanics. In: Proc 2nd Int Conf Numer Methods Geomech Blacksburg, Virginia, pp 132–150
- DeJong MJ (2009) Seismic assessment strategies for masonry structures—Ph.D. Thesis. Massachusetts Institute of Technology
- Dimitri R (2009) Stability of masonry structures under static and dynamic loads—Ph.D. Thesis. University of Salento
- Dimitri R, De Lorenzis L, Zavarise G (2011) Numerical study on the dynamic behavior of masonry columns and arches on buttresses with the discrete element method. *Eng Struct* 33:3172–3188
- Gabor D (1946) Theory of communication. *J Inst Electr Eng—Part III Radio Commun Eng* 93:429–441
- Housner G (1963) The behavior of inverted pendulum structures during earthquakes. *Bull Seismol Soc Am* 53:403–417
- Iervolino I, Cornell CA (2005) Record selection for nonlinear seismic analysis of structures. *Earthq Spectra* 21:685–713. doi:[10.1193/1.1990199](https://doi.org/10.1193/1.1990199)
- Iervolino I, Manfredi G, Cosenza E (2006) Ground motion duration effects on nonlinear seismic response. *Earthq Eng Struct Dyn* 35:21–38. doi:[10.1002/eqe.529](https://doi.org/10.1002/eqe.529)
- Ishiyama Y (1984) Motions of rigid bodies and criteria for overturning by earthquake excitations. *Bull New Zeal Soc Earthq Engineering* 17:24–37
- Itasca Inc. (2013) 3DEC 5.0: 3-Dimensional Distinct Element Code, Theory and Background
- Katsanos EI, Sextos AG (2013) ISSARS: an integrated software environment for structure-specific earthquake ground motion selection. *Adv Eng Softw* 58:70–85. doi:[10.1016/j.advengsoft.2013.01.003](https://doi.org/10.1016/j.advengsoft.2013.01.003)
- Katsanos EI, Sextos AG, Manolis GD (2010) Selection of earthquake ground motion records: a state-of-the-art review from a structural engineering perspective. *Soil Dyn Earthq Eng* 30:157–169. doi:[10.1016/j.soildyn.2009.10.005](https://doi.org/10.1016/j.soildyn.2009.10.005)

- Konstantinidis D, Makris N (2005) Seismic response analysis of multidrum classical columns. *Earthq Eng Struct Dyn* 34:1243–1270. doi:[10.1002/eqe.478](https://doi.org/10.1002/eqe.478)
- Lemos JV (2007) Discrete Element Modeling of Masonry Structures. *Int J Archit Herit* 1:190–213. doi:[10.1080/15583050601176868](https://doi.org/10.1080/15583050601176868)
- Leventakis G (2003) Microzoning of Thessaloniki. Ph.D. Thesis (in Greek)
- Manos G, Demosthenous M (1996) Study of the dynamic response of models of ancient columns or colonnades subjected to horizontal mase motions. In: 11th World Conf Earthq Eng
- Manos G, Petalas A, Demosthenous M (2013) Numerical and experimental study of the rocking response of unanchored body to horizontal base excitation. In: *Comput Methods Struct Dyn Earthq Eng COMP-DYN* 2013
- Marinelli A, Papanicolopulos SA, Kourkoulis S, Vayas I (2009) The pull-out problem in restoring marble fragments: a design criterion based on experimental results. *Strain* 45:433–444. doi:[10.1111/j.1475-1305.2008.00519.x](https://doi.org/10.1111/j.1475-1305.2008.00519.x)
- Mavroeidis G, Papageorgiou A (2003) Mathematical representation of near-fault ground motions. *Bull Seismol Soc Am* 93:1099–1131
- Mousavi M, Shahri M, Azarbakht A (2012) E-CMS: a new design spectrum for nuclear structures in high levels of seismic hazard. *Nucl Eng Des* 252:27–33. doi:[10.1016/j.nucengdes.2012.06.019](https://doi.org/10.1016/j.nucengdes.2012.06.019)
- Papaloizou L, Komodromos P (2009) Planar investigation of the seismic response of ancient columns and colonnades with epistyles using a custom-made software. *Soil Dyn Earthq Eng* 29:1437–1454. doi:[10.1016/j.soildyn.2009.06.001](https://doi.org/10.1016/j.soildyn.2009.06.001)
- Papantonopoulos C, Psycharis IN, Papastamatiou DY et al (2002) Numerical prediction of the earthquake response of classical columns using the distinct element method. *Earthq Eng Struct Dyn* 31:1699–1717. doi:[10.1002/eqe.185](https://doi.org/10.1002/eqe.185)
- Pappas A, da Porto F, Modena C (2016) Seismic vulnerability assessment form for free-standing columns based on a simplified numerical analysis. *Int J Archit Herit: Conserv Anal Restor*. doi:[10.1080/15583058.2015.1113336](https://doi.org/10.1080/15583058.2015.1113336)
- Pitilakis KD, Cultrera G, Margaritis B, et al. (2007) Thessaloniki seismic hazard assessment: probabilistic and deterministic approach for rock site conditions. In: 4th Int Conf Earthq Geotech Eng June 25–28. p 1701
- Psycharis IN, Papastamatiou DY, Alexandris AP (2000) Parametric investigation of the stability of classical columns under harmonic and earthquake excitations. *Earthq Eng Struct Dyn* 29:1093–1109. doi:[10.1002/1096-9845\(200008\)29:8<1093::AID-EQE953>3.0.CO;2-S](https://doi.org/10.1002/1096-9845(200008)29:8<1093::AID-EQE953>3.0.CO;2-S)
- Psycharis IN, Lemos JV, Papastamatiou DY, Zambas C, Papantonopoulos C (2003) Numerical study of the seismic behaviour of a part of the Parthenon Pronaos. *Earthq Eng Struct Dyn* 32:2063–2084
- Psycharis IN, Fragiadakis M, Stefanou I (2013) Seismic reliability assessment of classical columns subjected to near-fault ground motions. pp 2061–2079. doi:[10.1002/eqe](https://doi.org/10.1002/eqe)
- Rathje EM, Faraj F, Russell S, Bray JD (2004) Empirical relationships for frequency ground motions. *Earthq Spectra* 20:119–144. doi:[10.1193/1.1643356](https://doi.org/10.1193/1.1643356)
- Sehhati R, Rodriguez-Marek A, ElGawady M, Cofer WF (2011) Effects of near-fault ground motions and equivalent pulses on multi-story structures. *Eng Struct* 33:767–779. doi:[10.1016/j.engstruct.2010.11.032](https://doi.org/10.1016/j.engstruct.2010.11.032)
- Sextos AG, Katsanos EI, Manolis GD (2011) EC8-based earthquake record selection procedure evaluation: validation study based on observed damage of an irregular R/C building. *Soil Dyn Earthq Eng* 31:583–597. doi:[10.1016/j.soildyn.2010.10.009](https://doi.org/10.1016/j.soildyn.2010.10.009)
- Sextos AG, Nalmpantis S, Faraonis P, et al. (2013) Probabilistic seismic hazard assessment through geometrically non-linear back-analysis of Byzantine and Roman Monuments. In: 10th HSTAM Int Congr Mech Chania, Crete, Greece, pp 25–27
- Shome N, Cornell CA (1998) Normalized and scaling accelerograms for nonlinear structural analysis. In: *Proc 6th Natl Conf Earth-Quake Eng Seattle, WA*
- Shome N, Cornell CA (1999) Probabilistic seismic demand analysis of nonlinear structures. Reliability of marine structures. Department of Civil and Environmental Engineering, Stanford University, CA, CA
- Spanos P, Koh A (1984) Rocking of rigid blocks due to harmonic shaking. *J Eng Mech* 110:1627–1642
- Stewart JP, Shyh-Jeng Chiou, Graves RW, et al. (2001) Ground motion evaluation procedures for performance-based design—PEER report 2001/09
- Vassiliou MF, Makris N (2011) Estimating time scales and length scales in pulslike earthquake acceleration records with wavelet analysis. *Bull Seismol Soc Am* 101:596–618. doi:[10.1785/0120090387](https://doi.org/10.1785/0120090387)
- Yagoda-Biran G, Hatzor Y (2010) Constraining paleo PGA values by numerical analysis of overturned columns. *Earthq Eng Struct Dyn* 39:463–472
- Yim C, Chopra A, Penzien J (1980) Rocking response of rigid blocks to earthquakes. *Earthq Eng Struct Dyn* 8:565–587